

Study on Three-Dimensional Steady Vortex Structure in a Highly Loaded Compressor Cascade^{*}

ZHONG Jing-jun, KANG Da, LU Hua-wei, ZHANG Yong-chao

(Marine Engineering College, Dalian Maritime University, Dalian 116026, China)

Abstract: For further understanding the flow mechanism and vortex evolution law in a highly loaded compressor cascade, NACA65-010 blade profile with camber angle of 60° was selected. The formation, evolution and development of secondary flow vortices, including horse shoe vortex (HV), passage vortex (PV), concentrated shed vortex (CSV), corner vortex (CV) and so on, were analyzed with the method of topological analysis and numerical simulation. And the numerical method was validated by experimental results. The analysis shows that PV has the most impact on the flow field, and it turns to be stable structure in $130\%B$ section. The CV in the cascade passage are induced by PV, and the CV at outlet is induced by the combined action of PV and reverse flow from pressure surface to suction surface at outlet. Finally, the flow structure in cross section presents a profile of coexistence of PV with CSV. In the end, a vortex structure at incidence of 0° was provided.

Key words: Compressor cascade; Vortex structure; Topological analysis; Secondary flow

CLC number: V231.1 **Document code:** A **Article number:** 1001-4055 (2015) 06-0852-12

DOI: 10.13675/j. cnki. tjjs. 2015. 06. 008

高负荷扩压叶栅三维定常旋涡结构建模研究

钟兢军, 康 达, 陆华伟, 张永超

(大连海事大学轮机工程学院, 辽宁大连 116026)

摘 要: 为进一步认识高负荷扩压叶栅内的流动机理和旋涡演变规律, 采用经试验校核的数值方法, 以具有 60° 折转角的 NACA65-010 叶型为研究对象, 运用拓扑分析理论, 探讨了叶栅流道内马蹄涡、通道涡、集中脱落涡和壁角涡等二次旋涡的生成、演绎与发展。分析认为, 在高负荷扩压叶栅中, 对流场影响最大的涡系结构为通道涡, 通道涡在 $130\%B$ 截面转变为稳定的内旋结构, 流道内的壁角涡由通道涡诱导形成, 而出口角涡则是在叶片尾缘出口绕流与通道涡的综合作用下形成的, 流场出口最终呈现出通道涡与集中脱落涡并存的稳定结构。最后给出了 0° 冲角下的三维旋涡结构示意图。

关键词: 扩压叶栅; 旋涡结构; 拓扑分析; 二次流

Nomenclature

B: axial chord-wise

PV: passage vortex

CVP: the corner vortex of pressure side

CVS: corner vortex of suction side

CV: corner vortex

CSV: concentrated shed vortex

HVP: pressure leg of horse shoe vortex

HVS: suction leg of horse shoe vortex

SV: trailing edge shedding vortex

* 收稿日期: 2014-05-08; 修订日期: 2014-06-25。

基金项目: 国家自然科学基金 (51206013, 51436002); 高等学校博士学科点专项科研基金 (20112125120009); 中央高校基本科研业务专项资金 (3132015026)。

作者简介: 钟兢军 (1963—), 男, 博士, 教授, 研究领域为叶轮机械气动热力学。E-mail: zhongjj@dlmu.edu.cn

通讯作者: 陆华伟 (1980—), 男, 博士, 副教授, 研究领域为叶轮机械气动热力学。E-mail: hwlu66@163.com

1 Introduction

Various concentrated vortices may emerge during gas flow through compressor cascade, including horse shoe vortex, passage vortex, concentrated shed vortex and corner vortex and so on. The characteristics of the whole flow field are under the domination of the formation, evolution and development of the secondary flow vortices^[1]. As the load of the compressor improving, the internal flow presents significant three-dimensional characteristics, as the percentage of secondary flow loss going higher. In order to uncover the mechanism of the internal flow in a highly loaded compressor cascade, the vortices as well as the interactive relationships of them were analyzed and discussed in this paper. And it is necessary to have a clear grasp of the detailed flow structure for the study on the mechanism of the internal flow. With the continued perfection of qualitative resolution of differential equation, the topology theory used in qualitative analyses of flow patterns is developing rapidly. This method can describe explicitly the three-dimensional separation configuration and the vortex structure^[2]. Topological analysis has been successfully used in external flow field, for instance, the application in research about the formation and development of the multiple vortices around a wing strongly promoted the wing design theory. The results of research on external flow are worthy of learning. Professor KANG^[3] established a series of topological rules adapting for turbomachinery, and discussed the flow patterns of compressor cascades in detail. Professor WANG^[4] pointed that, compared with a stable passage vortex, the loss caused by an unstable passage vortex or a passage vortex restricted by a stable limit cycle was much more. LU^[5] et al. conducted a detailed study on the flow field structure in a low speed compressor stator passage with hub tip. YU^[6] et al. discussed the evolution of the rotor tip leakage vortex under design condition, and gave the mechanism of the instability and broken of the leakage vortex. ZHAO^[7] built a vortex model for a Controlled Diffusion Airfoil highly loaded compressor cascade with the method of topological analysis. Series of experiments to investigate the vortical flow in compressor cascades were conducted by TANG^[8].

So far, there are fewer results on compressor vortex

models than on turbine vortex models^[9-10], and the discussions on highly loaded compressor vortex models are much less^[11-15]. Numerical study and topological analysis about a highly loaded compressor cascade vortex structure were presented in this paper, and the numerical method was validated by experimental results. As the separation flow in highly loaded compressor cascade is very serious, both experimental method and numerical method have difficulty exploring the flow field in the flow passage, especially for the off-designed conditions. Hence, only the topological analysis at incidence of 0° was provided. We hope that this paper can contribute to deepening the understanding about the mechanism of evolution and distribution of vortices in a highly loaded compressor cascade.

2 Computation Procedure and Its Validation

Selecting NACA65-010 (shown in Fig.1) compressor profile as the research object, its main parameters are described in Table 1. Numerical simulation was conducted based on NUMECA software with the same geometry and boundary conditions as those in the experimental research. The boundary conditions are inlet relative total pressure of 630.7 Pa, inlet total temperature of 305.7 K, incidence of 0° , outlet relative static pressure of 0 Pa and the reference pressure of 101734.7 Pa. The incoming boundary layer thickness is 10 mm. During the computation, the two-equation turbulence model $k-\varepsilon$ (EWF) of low Reynolds number was adopted. The applied computation grid (shown in Fig.2) with the topology of H-O-H type consists of 1201054 nodes. The near-wall grid was densified to meet the requirement of y^+ , and the grid's y^+ is less than 3. For the sake of reliability of the simulation, experiments of measurement about outlet flow field and oil flow visualization were carried out in a low-speed wind tunnel at Dalian Maritime University. The inlet Reynolds number based on the inlet velocity and blade chord is 3.2×10^5 . A five-hole probe was used for the measurement of flow field in 160% B section. Its detailed procedure can be referenced in ref[16]. By the comparison (shown in Fig.3 ~ Fig.6) of simulated results with the measured data, it is found that the calculated results have a good agreement with the experimental data both in aspects of quality and

quantity, so the accuracy of the numerical method is verified.

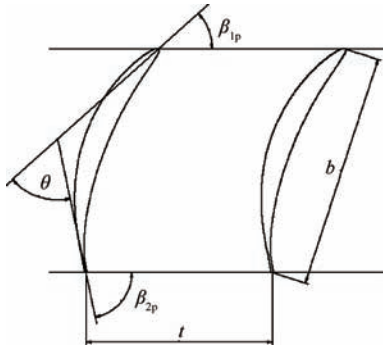


Fig. 1 Cascade geometry parameters

Table 1 Parameters of blade profile

Stagger angle	Inlet angle β_{1p}	Outlet angle β_{2p}	Camber angle θ	Pitch t	Chord b	Blade span	D
18.05°	41.95°	101.95°	60°	95mm	120mm	160mm	0.5

3 Results and discussion

3.1 Topological analysis of secondary flow in sections

Secondary streamline and topological structure in

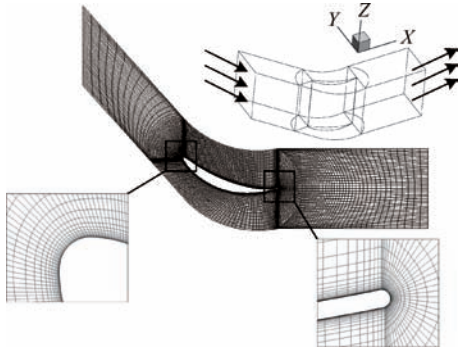
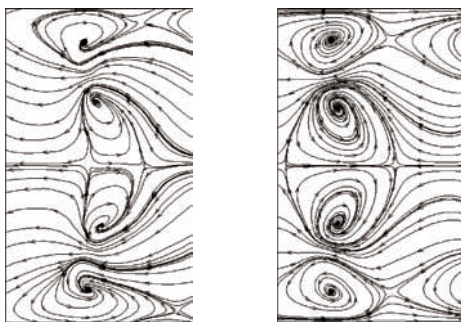


Fig. 2 Grid for calculation



(a) Experimental (b) Numerical

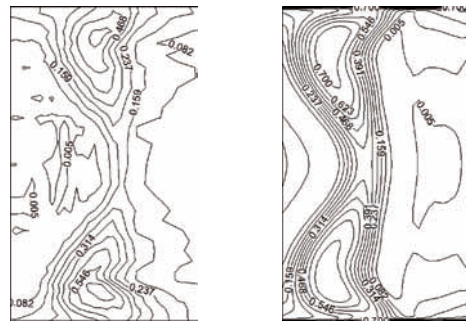
Fig. 3 Contrast of experimental results and numerical results about secondary flow in 160%B section

cross sections of every other 10%B are shown in Fig.7 to

Fig.9, and the orientation of average flow angle in every section was defined as the primary flow direction. The flow image in every section is horizontally symmetry, so just the bottom half of flow fields are given. According to ref.[17], singular points of sections intersected with both pressure surface and suction surface obey the topology rule

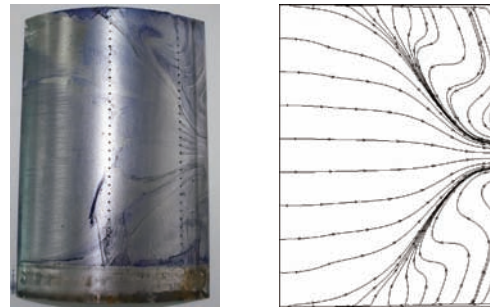
$$\sum N + 0.5 \sum N' - \sum S - 0.5 \sum S' = 1 \quad (1)$$

(N and S means node point and saddle point, N' and S' means semi-node point and semi-saddle point), while the other sections have no such constraint.



(a) Experimental (b) Numerical

Fig. 4 Contrast of experimental results and numerical results about loss distribution in 160%B section



(a) Experimental (b) Numerical

Fig. 5 Contrast of experimental results and numerical results about limiting streamlines on SS

3.1.1 Sections before cascade inlet

The section shown in Fig.7(a) locates in front of leading edge at a distance of 10%B, the topological structure in this section is simple due to the incoming flow is steady. Observed from Fig.7(b), at the corner of pressure/hub semi-node N_1' (see Fig.7(a)) rises from the endwall and transforms into node N_1 , N_1 is linked with N_2 by saddle point S_1 , S_1 and S_{m1} are connected by

node point N_2 . There is no helix structure in both of the sections.

3.1.2 Sections inside cascade passage

In Fig.8(a), close to the corner of pressure/hub appear two vortex cores, N_3 and N_4 . N_4 represents PV at the beginning of formation, and the low energy fluid at the corner of pressure/hub turns to be CVP under the induction of PV. Professor ZHANG^[18] pointed that $\lambda =$

$(1/\rho_0)(\partial\rho\omega/\partial z)_0$ was an important parameter determining the low speed vortex evolution along axial direction. When $\lambda > 0$, the secondary flow fluid around vortex core spirals from outside to inside, then the vortex is a stable spiral; otherwise ($\lambda < 0$), the vortex is an unstable spiral. Because of the positive pressure gradient near pressure side, PV appears to be a stable vortex structure. CVP is unstable because the low energy fluid is continu-

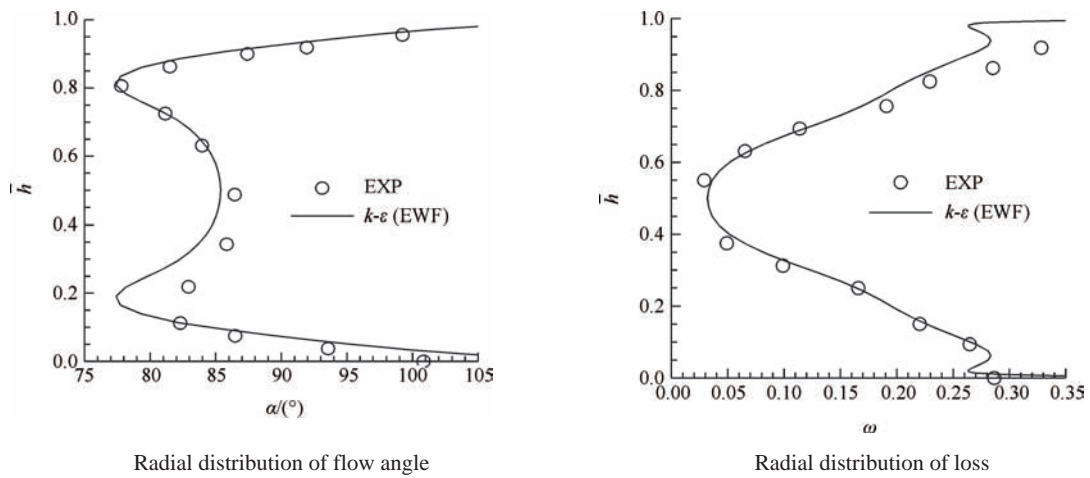


Fig. 6 Contrasts of experimental results and numerical results about radial distribution of parameters

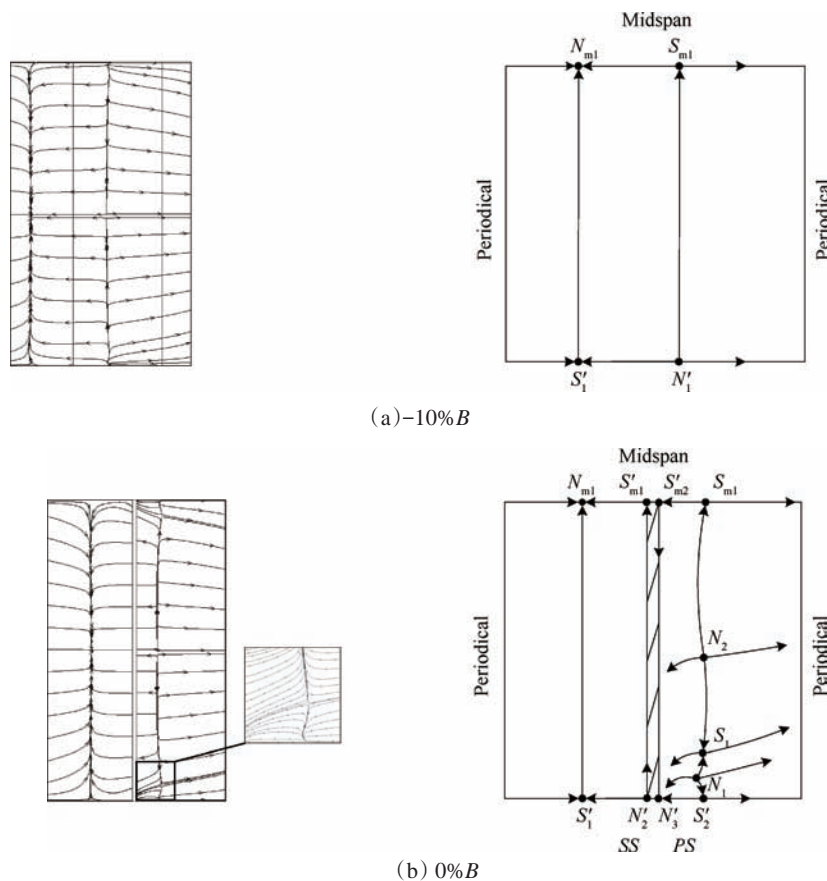


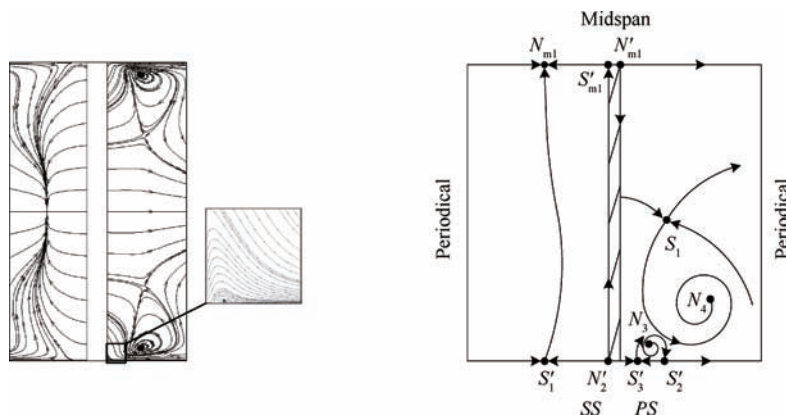
Fig. 7 Secondary flow and topological structure in sections before cascade inlet

ally transported from pressure side to suction side by intense traverse secondary flow on endwall. And there is no significant change in topological structure near the side of suction surface in Fig.8(a). The topological structure in Fig.8(b) has little change compared with the previous one, PV and CVP expand in scale, and PV moves toward suction side under the action of traverse pressure gradient. Seen from Fig.8(c), PV expands in scale further, the saddle point S_1 (see Fig.8(b)) has been pushed into midspan and then converted into the saddle point S_{m3} , an unstable spiral node point N_5 denoting CVS emerges at the corner of suction/hub in 30%B section, CVP approaches pressure side with the expansion of PV. The semi-saddle point S_5' in Fig.8(c) indicates that CVP begins to obtain vorticity from pressure surface. The adverse pressure gradient gradually increases along the flow direction, and strong adverse pressure gradient is unfavorable for PV to maintain stable structure, therefore, PV presents an unstable spiral in 40%B section (see Fig.8(d)). In Fig.8(d), CVS turns to be a stable spiral due to the low energy fluid transported by traverse secondary flow to deposit at the corner of suction/hub. Observed from Fig.8(e), the vortex core (node point N_4) of PV has been driven to suction side by traverse pressure gradient in 50%B section, the CVP's outer fluid turns round out of its core and its configuration becomes long and narrow under the influence of PV. At the corner of pressure/hub, the low energy fluid is carried away by traverse secondary flow on endwall, and meanwhile, high energy fluid is continuously induced by PV to inject into the corner. Hence, it's difficult for CVP to

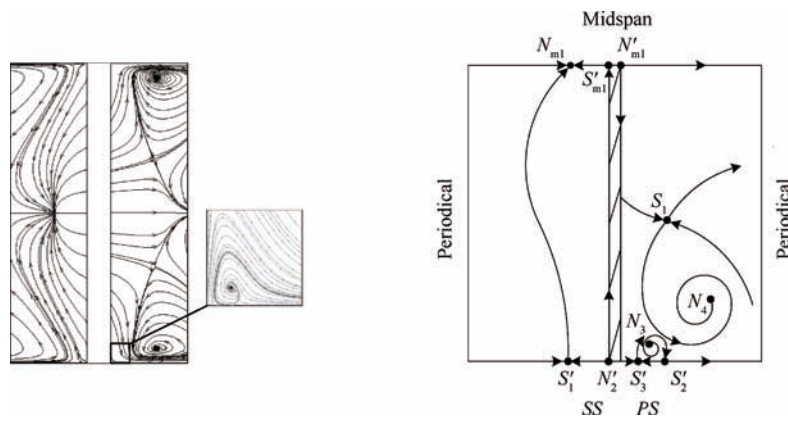
keep a stable spiral. During the process of topological structure transition, the vortex core converts to be unstable status firstly, but its outer fluid is unable to perceive the transformation immediately, so CVP is surrounded by a stable limit cycle in Fig.8(f). As for the topological structure in 70%B section (see Fig.8(g)), CVP has disappeared and CVS apparently becomes weak. In Fig.8(h), the topological structure in 80%B section almost inherits the features from the last section. In Fig.8(i), the vortex core of PV divides into two spiral nodes (N_4 and N_7), and N_4 is linked with N_7 by saddle point S_6 .

3.1.3 Sections behind cascade outlet

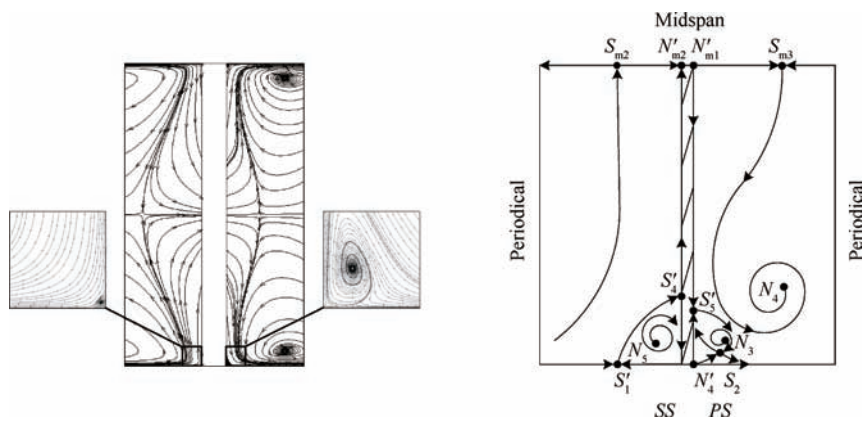
At cascade outlet shown in Fig.9(a), N_4 and N_7 roll into one, CVS converts to be a reattachment node point N_5 due to the reverse flow from pressure side, a new spiral node N_8 denoting CV emerges at the corner of pressure/hub. It is clear that CVP vanished in 70%B section (see Fig.8(g)), so CV and CVP are not related. CV is formed under the interaction between PV and the wake flow from pressure side to suction side driven by pressure gradient across blade trailing. In Fig.9(b), near the midspan appear a degradation node point N_9 , which gathers the fluid from wake, mainstream and endwall layer, and CV grows stronger in 110%B section. In Fig.9(c), CV gradually dissipates with the formation of principal vortex structure. In Fig.9(d), the degradation node point N_9 is changed to be a spiral node point which represents CSV, and CV completely disappears. It's worth noting that, in 130%B section PV turns into a stable spiral due to the vanishing of adverse pressure gradient. Observed from Fig.9(e) and Fig.9(f), the flow structure



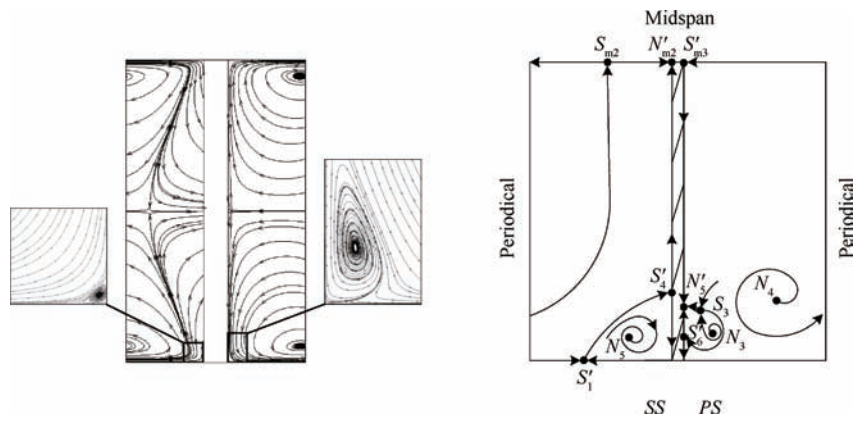
(a) 10%B



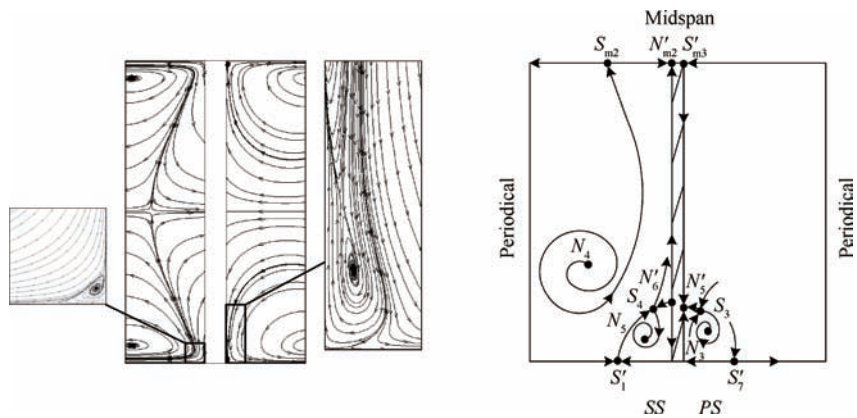
(b) 20%B



(c) 30%B



(d) 40%B



(e) 50%B

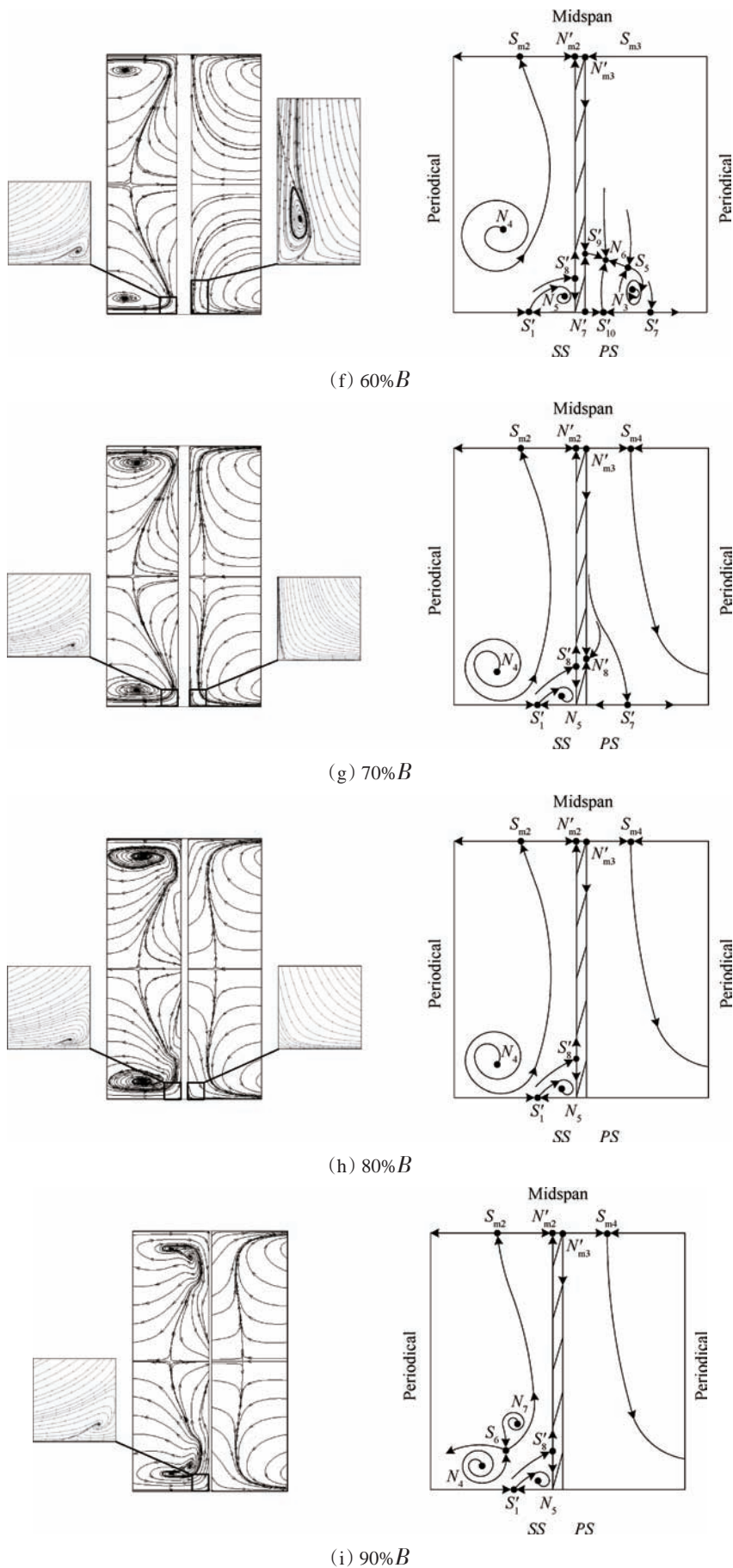


Fig. 8 Secondary flow and topological structure in sections inside cascade inlet

stops changing and presents a profile of coexistence of passage vortex with concentrated shed vortex.

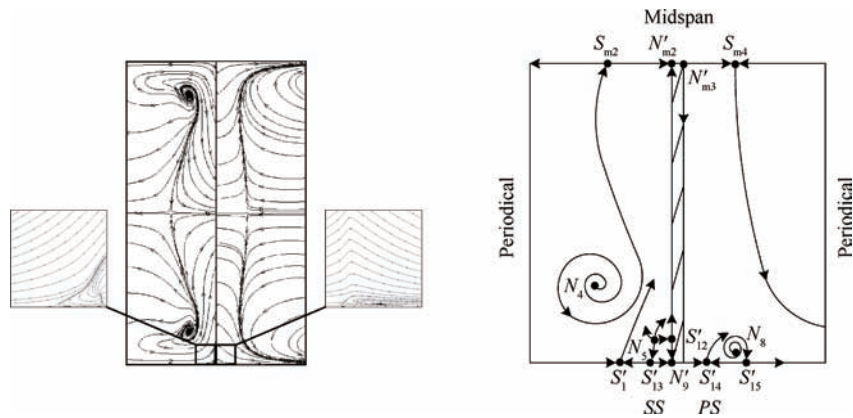
3.1.4 The change rule of the amount of singular points along axial direction

In order to investigate the change rule of the amount of singular points along axial direction, the amount of singular points is defined as:

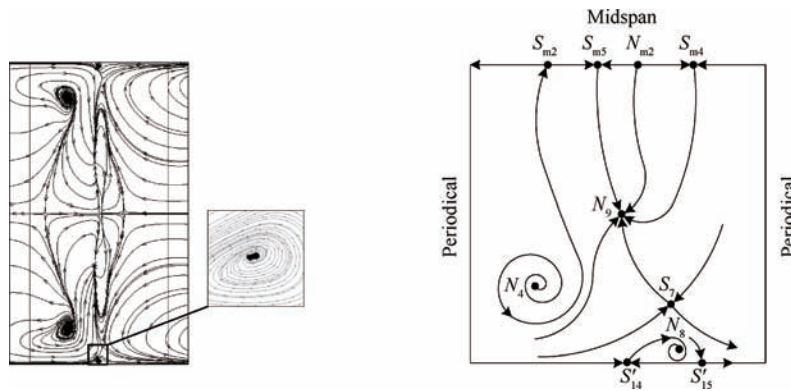
$$N_{sp} = \sum N + \sum S + 0.5(\sum N' + \sum S') \quad (2)$$

The change rule is shown in Fig.10. There are only four singular points before cascade inlet, then N_{sp} in-

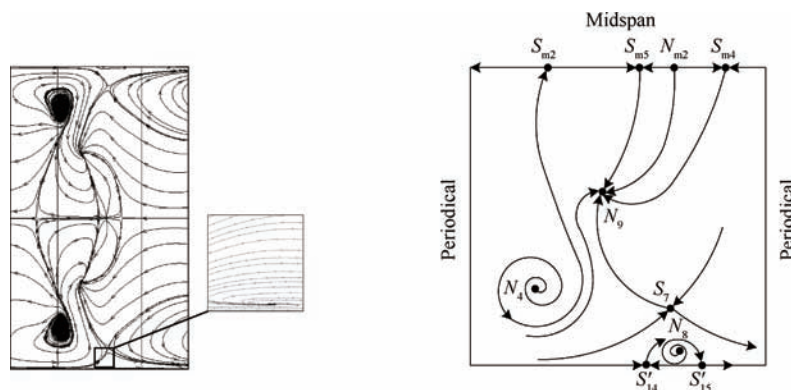
creases rapidly after fluid getting into the passage due to the continuous forming of vortices. The amount of singular points reaches a maximum of 18 in 60% B section which contains three vortex motions (PV, CVS and CVP). After then, N_{sp} reveals a trend of sharp decrease for the vanish of CVP. The fluid from both sides of the blade mix at cascade outlet, therefore N_{sp} creeps back up to 15 in 100% B section. After the formation of principal vortices, and the mixture process is complete, N_{sp} declines to 8 and maintains at that level.



(a) 100%B



(b) 110%B



(c) 120%B

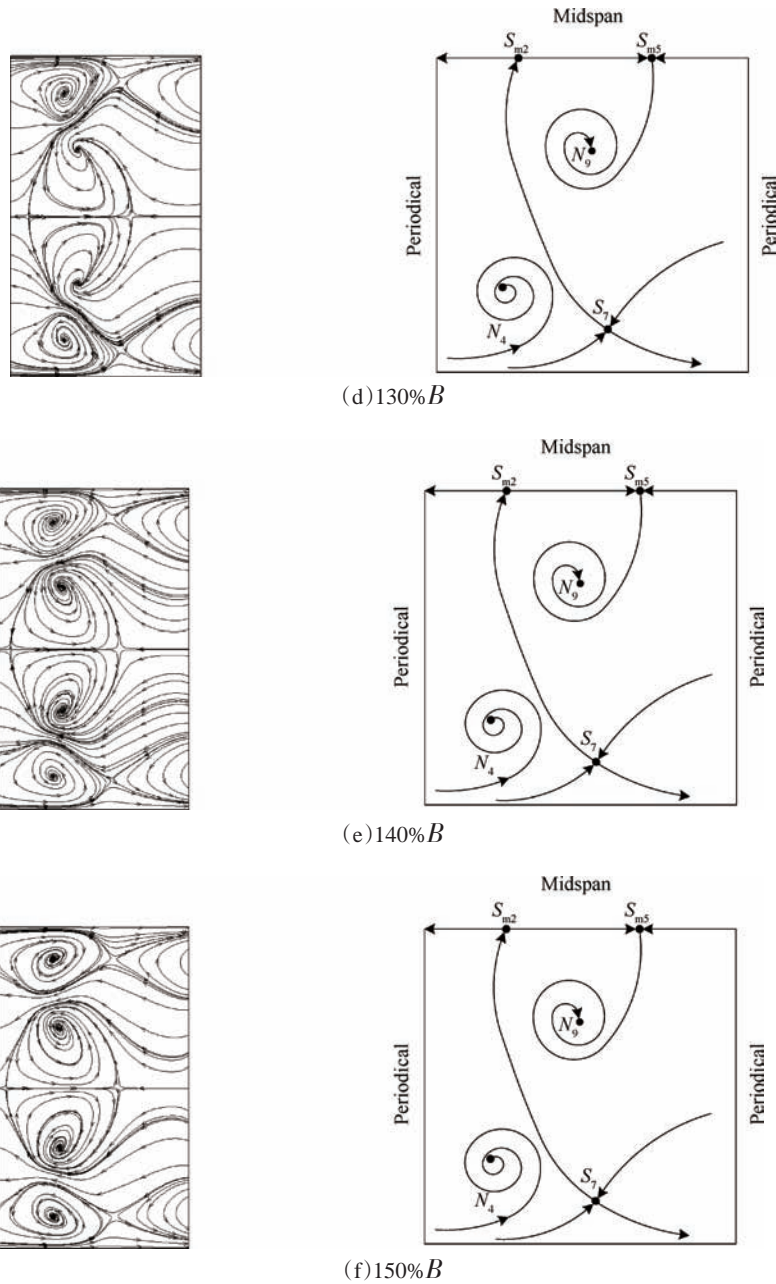


Fig. 9 Secondary flow and topological structure in sections behind cascade outlet

3.2 Topological analysis of limiting streamlines on solid surface

According to the theory of vorticity dynamics, boundary layer with high concentrated vorticity forms when gas flows over static solid surface. The boundary layer approaches separation line and then rolls up into vortex. Hence, it's sure that the vortex is accompanied by the separation line. Streamlines on sections extremely near solid surface have the same direction as the wall shear stress field. The solid surface topological structure

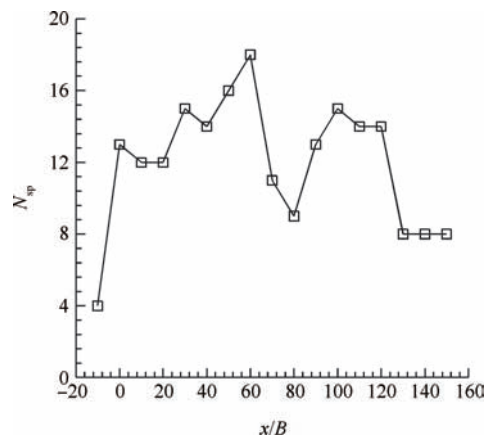


Fig. 10 Change rule of the amount of singular points along axial direction

(shown in Fig.12) is given on the basis of limiting streamlines (shown in Fig.11).

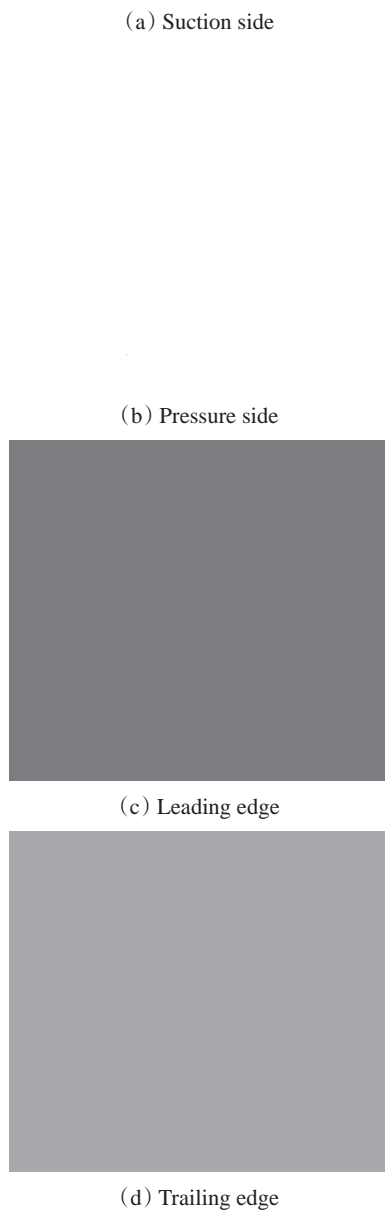


Fig. 11 Limiting streamlines on solid surface

In Fig.12, four reattachment lines radiate from the leading edge node N_m , two of them intersect at the trailing edge saddle S_m , the other two stretch along spanwise

direction into the leading edge saddle S_{l1} . Static pressure of incoming flow in every part of the same cross section is nearly equal, but the total pressure in boundary layer on endwall is lower. Therefore, fluid flows toward endwall after stagnating at leading edge, then reattachment node N_{h1} forms on hub near leading edge. N_{h1} is connected by S_{l1} to N_m . Two separation lines on endwall H_p and H_s start at saddle point S_{h1} , H_p and H_s denotes HVP and HVS, respectively. Limiting streamlines beside H_p and H_s are almost parallel with H_p and H_s , so HVP and HVS are unable to be revealed by secondary flow image. Two opposite direction reattachment lines from N_{h1} and N_{s1} encounter at saddle point S_{s1} . Under the action of adverse pressure gradient on suction surface, streamlines originates from N_{s1} move toward N_{l1} along the suction separation line $S_{s1} \rightarrow N_{l1}$. The boundary layer fluid on endwall separates from $N_{h2} \leftarrow S_{h2} \rightarrow N_{h4}$, and then reattaches on suction surface along the reattachment line $S_{s1} \leftarrow N_{s1} \rightarrow S_{s2}$ at the corner of suction/hub. $S_{h2} \rightarrow N_{h4}$ is the separation line of the corner vortex of suction side. There is one separation line at the corner of pressure/hub, $S_{l1} \rightarrow N_{p1}$, which is the separation line of the corner vortex of pressure side. CVP reattaches on endwall along the reattachment line $N_{h1} \rightarrow S_{h3}$. At cascade outlet, the mixing of fluid from both sides of the blade makes the topological structure near trailing edge quite complicated. The exit fluid of pressure side flows round the trailing edge and then acts on suction surface, therefore reattachment node N_{s2} emerges on suction surface near trailing edge. One part of the reattached fluid moves toward N_{l1} along the separation line $S_{s2} \rightarrow N_{l1}$, the other part enters into boundary layer on endwall. The low energy fluid in corner region near trailing edge gets into outer fluid from the two opposite spiral node, N_{h4} and N_{h5} . The attached eddy layer on pressure and suction surfaces shed from the trailing edge separation line $S_m \rightarrow N_{l1}$ and forms the spanwise SV. The limiting streamlines on pressure surface gradually deflect toward endwall along the flow direction. As the fluid at the corner of pressure/hub is continually transported from pressure side to suction side by traverse secondary flow, fluid on pressure surface near hub moves toward endwall to replenish fluid in corner region. Besides, the expansion of gas at out-

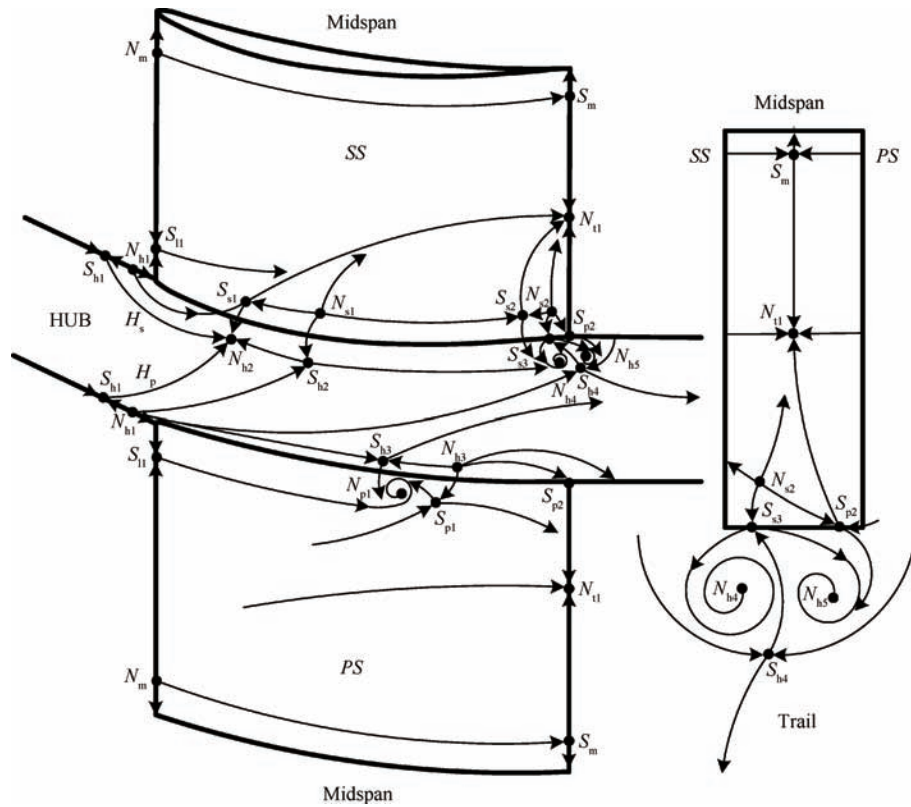


Fig. 12 Solid surface topological structure

let intensifies the deflection. One reattachment node N_{h3} at the corner of pressure/hub forms due to the fluid deflection. One separation line originates from S_{h4} and extends downstream, which is the separation line of corner vortex at outlet. There are 19 nodes and 21 saddles in the whole passage of cascade, $\sum N - \sum S = -2$, the number of singular points conforms with the topological law^[17].

3.3 Three-dimensional vortex structure

The three-dimensional vortex structure inside passage of cascade is presented in Fig.13 according to the analysis above. The incoming boundary layer is incised by leading edge and forms the two legs (HVP and HVS) of horse shoe vortex. HVP gradually thrives to be PV along the flow direction. HVS dissipates and disappears at the corner of suction/hub. The low energy fluid in corner region is induced to be CVP and CVS by PV. CV at outlet forms under the interaction between PV and the wake flow from pressure side to suction side. At cascade outlet, part of the mainstream and boundary layer from hub and blade surfaces coil into CSV. The attached eddy layer on blade surfaces shed from the trailing edge and forms the spanwise SV.

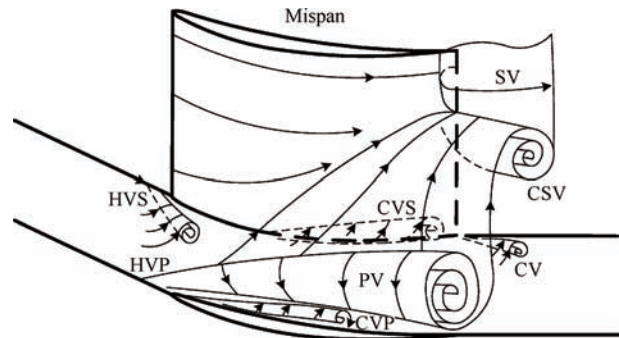


Fig. 13 Sketch of the vortex structure

4 Conclusions

(1) The study indicates that numerical results are consistent with the experimental data both in aspects of quality and quantity.

(2) At the simulation conditions of this paper, there are seven vortices in the flow passage, including HVP, HVS, PV, CVP, CVS, CV and SV. Among all the vortices, PV has the most powerful effect on the flow field. PV presents an unstable spiral structure in most region in the flow passage due to the adverse pressure gradient, and it turns to be stable structure in 130%B section as adverse pressure gradient vanishes.

(3) The low energy fluid in the corner region roll

up into CVP and CVS under the induction of PV.CV at outlet forms under the combined action of PV and the wake flow from pressure surface to suction surface.

References:

- [1] 张华良,王松涛,王仲奇. 冲角对压气机叶栅内二次涡的影响[J]. 航空动力学报, 2006, 21(1):15-155.
- [2] ZHANG Yong-jun, WANG Hui-she, XU Jian-zhong, et al. Study on Topology and Vortex Structure in a Diffusion Cascade [J]. *Science in China Series E*, 2009, 52(8):2305-2315.
- [3] KANG Shun. Investigation on the Three-Dimensional Flow within a Compressor Cascade with and without Tip Clearance[D]. *Brussels: Vrije University Brussels*, 1993.
- [4] 王松涛,吴 猛,王仲奇,等. 通道涡稳定性及对损失的影响[J]. 工程热物理学报, 2000, 21(4):425-429.
- [5] 陆华伟,郭 爽,钟兢军,等. 带根部间隙压气机静叶流道流动结构研究[J]. 工程热物理学报, 2012, 33(1):51-54.
- [6] 于宏军,刘宝杰,刘火星,等. 设计状态下压气机转子叶尖泄漏涡流动研究[J]. 航空学报, 2004, 25(1):1-8.
- [7] ZHAO Xiao-hu, LI Ying-hong, WU Yun, et al. Numerical Investigation of Flow Separation Control on a Highly Loaded Compressor Cascade by Plasma Aerodynamic Actuation [J]. *Chinese Journal of Aeronautics*, 2012, 25(3):349-360.
- [8] 周 逊,韩万金. 涡轮矩形叶栅中的旋涡模型的进展回顾[J]. 航空动力学报, 2001, 16(3):199-204.
- [9] 唐燕平,陈懋章,陈 芳. 扩压叶栅中的旋涡流动[J]. 航空动力学报, 1990, 5(2):103-186.
- [10] Inoue M, Kuroumarou M. Three-Dimensional Structure and Decay of Vortices Behind and Axial Flow Rotation Blade Row [J]. *Journal of Engineering for Gas Turbines and Power-Transactions of the ASME*, 1984, 106(3):561-569.
- [11] 郭 爽,陆华伟,宋彦萍,等. 端壁附面层抽吸对大转角扩压叶栅旋涡影响的实验研究[J]. 推进技术, 2013, 34(11):1466-1473. (GUO Shuang, LU Hua-wei, SONG Yan-ping, et al. Experimental Investigation on Effects of Endwall Boundary Layer Suction on Vortexes of High-Turning Compressor Cascades [J]. *Journal of Propulsion Technology*, 2013, 34(11):1466-1473.)
- [12] 陈 浮,陈绍文,郭 爽,等. 高负荷压气机叶栅分离与流场结构研究[J]. 工程热物理学报, 2008, 29(1):49-51.
- [13] GUO Shuang, LU Hua-wei, CHEN Fu, et al. Vortex Control and Aerodynamic Performance Improvement of a Highly Loaded Compressor Cascade via Inlet Boundary Layer Suction [J]. *Experiments in Fluids*, 2013, 54:1570.
- [14] GUO Shuang, CHEN Shao-wen, LU Hua-wei, et al. Enhancing Aerodynamic Performance of a High-Turning Compressor Cascade via Boundary Layer Suction[J]. *Science in China Series E*, 2010, 53(10):2748-2755.
- [15] 王学德,赵小虎,王路成. 高负荷压气机叶栅等离子体流动控制数值仿真与拓扑分析[J]. 推进技术, 2013, 34(10):1321-1329. (WANG Xue-de, ZHAO Xiao-hu, WANG Lu-cheng. Numerical Investigation and Topological Analysis of Plasma Flow Control on a Highly Loaded Compressor Cascade [J]. *Journal of Propulsion Technology*, 2013, 34(10):1321-1329.)
- [16] ZHONG Jing-jun, HAN Shao-bing, LU Hua-wei, et al. Effect of Tip Geometry and Tip Clearance on the Aerodynamic Performance of a Linear Compressor Cascade [J]. *Chinese Journal of Aeronautics*, 2013, 26(3):583-593.
- [17] KANG Shun. An Application of Topological Analysis to Studying the Three-Dimensional Flow in Cascades: Part I-Topological Rules for Skin-Friction Lines and Section Streamlines [J]. *Applied Mathematics and Mechanics*, 1990, 11(5):489-495.
- [18] 张涵信. 旋涡沿轴线的非线性分叉[J]. 空气动力学学报, 1994, 12(3):243-251.

(编辑:刘萝威)